40. Shah S, Hecht A, Pestell R, Byers SW. Trans-repression of beta-catenin activity by nuclear receptors. J Biol Chem 2003;278: 48137–45.
41. Kitareewan S, Blumen S, Sekula D, Bissonnette RP, Lamph WW, Cui Q, et al. G0S2 is an all-trans-retinoic acid target gene. Int J Oncol 2008;33:397–404.
42. Uray IP, Shen Q, Seo HS, Kim H, Lamph WW, Bissonnette RP, et al. Rexinoid-induced expression of IGFBP-6 requires RARbeta-dependent permissive cooperation of retinoid receptors and AP-1. J Biol Chem 2009;284:345–53.
43. Hough S, Avioli LV, Muir H, Gelderblom D, Jenkins G, Kurasi H, et al. Effects of hypervitaminosis A on the bone and mineral metabolism of the rat. Endocrinology 1988;122: 2933–9.
44. Ribaya-Mercado JD, Blumberg JB. Vitamin A: is it a risk factor for osteoporosis and bone fracture? Nutr Rev 2007;65: 425–38.
45. Llovet JM, Ricci S, Mazzaferro V, Hilgard P, Gane E, Blanc JF, et al. Sorafenib in advanced hepatocellular carcinoma. N Engl J Med 2008;359:378–90.
46. Okita K, Matsui O, Kumada H, Tanaka K, Kaneko S, Moriwaki H, et al. Effect of peretinoin on recurrence of hepatocellular carcinoma (HCC): results of a phase II/III randomized placebo-controlled trial. J Clin Oncol 2010;28 Suppl 15s:4024.

Hypervascular Hepatocellular Carcinoma: Correlation between Biologic Features and Signal Intensity on Gadoxetic Acid–enhanced MR Images

Azusa Kitao, MD
Osamu Matsui, MD
Norihide Yoneda, MD
Kazuto Kozaka, MD
Satoshi Kobayashi, MD
Wataru Koda, MD
Toshifumi Gabata, MD
Tatsuya Yamashita, MD
Shuichi Kaneko, MD
Yasuni Nakanuma, MD
Ryuichi Kita, MD
Shigeki Arii, MD

Purpose: To analyze the correlation among biologic features, tumor marker production, and signal intensity at gadoxetic acid–enhanced MR imaging in hepatocellular carcinomas (HCCs).

Materials and Methods: Institutional ethics committee approval and informed consent were obtained for this retrospective study. From April 2008 to September 2011, 180 surgically resected HCCs in 180 patients (age, 65.0 years ± 10.3 [range, 34–83 years]; 138 men, 42 women) were classified as either hypointense (n = 158) or hyperintense (n = 22) compared with the signal intensity of the background liver on hepatobiliary phase gadoxetic acid–enhanced MR images. Pathologic features were analyzed and α fetoprotein (AFP) and protein induced by vitamin K absence or antagonist-II (PIVKA-II) production were compared by means of serum analysis and immunohistochemical staining. Recurrence and survival rates were also evaluated. The Mann-Whitney and Pearson correlation tests were used for statistical analysis.

Results: The grade of differentiation was higher (P = .028) and portal vein invasion was less frequent in hyperintense HCCs (13.6%) than in hypointense HCCs (36.7%) (P = .039). The serum levels of AFP, *Lens culinaris* agglutinin reactive fraction of AFP, and PIVKA-II were lower in hyperintense than in hypointense HCCs (P = .003, .004, and .026, respectively). Immunohistochemical AFP and PIVKA-II expression were lower in hyperintense than in hypointense HCCs (both $P < .001$). The recurrence rate was lower in hyperintense than in hypointense HCCs (P = .039).

Conclusion: The results suggest that hyperintense HCCs on gadoxetic acid–enhanced MR images are less aggressive than hypointense HCCs.

Supplemental material: *http://radiology.rsna.org/lookup/suppl/doi:10.1148/radiol.12120226/-/DC1*

[1] From the Departments of Radiology (A.K., O.M., N.Y., K.K., S. Kobayashi, W.K., T.G.), Gastroenterology (T.Y., S. Kaneko), and Human Pathology (Y.N.), Kanazawa University Graduate School of Medical Science, 13-1 Takaramachi, Kanazawa 920-8640, Japan; Department of Gastroenterology, Osaka Red Cross Hospital, Osaka, Japan (R.K.); and Department of Hepatobiliary-Pancreatic Surgery, Tokyo Medical and Dental University, Tokyo, Japan (S.A.). Received February 9, 2012; revision requested March 27; revision received April 24; accepted May 17; final version accepted June 29. Supported in part by a Grant-in-Aid for Scientific Research (21591549) from the Ministry of Education, Culture, Sports, Science and Technology; and by Health and Labor Sciences Research Grants for "Development of novel molecular markers and imaging modalities for earlier diagnosis of hepatocellular carcinoma." **Address correspondence to** A.K. (e-mail: *kitaoa@staff.kanazawa-u.ac.jp*).

Hepatocellular carcinoma (HCC) is the most frequent primary malignant hepatic tumor and the third most common cause of cancer death worldwide (1). The accurate detection and characterization of HCC are critical issues in clinical practice for improving the prognosis of patients with HCC.

Gadoxetic acid–enhanced MR imaging is a new imaging modality with high accuracy for diagnosing HCCs (2–4). On images obtained during the hepatobiliary phase of gadoxetic acid–enhanced MR imaging, HCCs commonly show hypointensity when compared with the background liver. However, approximately 6%–15% of hypervascular HCCs demonstrate iso- or hyperintensity, which is uncommon among hepatic malignant tumors (5–8). This hyperintensity was previously shown to be due to overexpression of organic anion transporting polypeptide 8 (OATP8, synonymous with OATP1B3), which might be the uptake transporter of gadoxetic acid in HCCs (5,6). In the normal liver, OATP8 is expressed on the sinusoidal side of the hepatocyte membrane and takes up many intrinsic and extrinsic organic anions from blood into hepatocytes.

On the other hand, Jung et al (9) showed that OATP8 was up-regulated by hepatocyte nuclear factor 1α. These hepatocyte nuclear factors are indispensable transcription factors that relate to primitive embryonal differentiation of hepatocytes and to hepatocarcinogenesis. We suspected that these atypical hypervascular HCCs that show hyperintensity on hepatobiliary phase images (hyperintense HCC) might reflect a distinct subtype of HCC with a particular molecular background and biologic features.

The main tumor marker of HCCs is α-fetoprotein (AFP), especially the *Lens culinaris* agglutinin reactive fraction (L-3). Similarly, the protein induced by vitamin K absence or antagonist-II (PIVKA-II) is a clinically important serum tumor marker. PIVKA-II is an incomplete coagulation factor prothrombin II whose production is related to the absence of vitamin K or the presence of the antagonist of vitamin K, which is the cofactor of γ carboxylase that converts precursor into prothrombin (10). Serum levels of both AFP and PIVKA-II correlate with the histologic degree of malignancy and the prognosis in HCC (11). In addition, there are reports (12,13) showing that AFP expression in HCCs is regulated by several enhancers and suppressors, including the hepatocyte nuclear factor family. Although the molecular basis of PIVKA-II production is not well explained, we speculated that there might be a correlation of the tumor marker production and signal intensity (SI) on hepatobiliary phase images, which would reflect distinct genomic and proteomic expression of HCC.

The purpose of this study was to analyze the correlation among the pathologic and biologic features, tumor marker production, with SI on hepatobiliary phase gadoxetic acid–enhanced MR images of HCCs.

Advances in Knowledge

- Hypervascular hepatocellular carcinomas (HCCs) that hyperintensity relative to the surrounding liver on hepatobiliary phase gadoxetic acid–enhanced MR images demonstrate a significantly higher grade of differentiation ($P = .028$) and rarer portal vein invasion ($P = .039$) than those of hypointense HCCs.
- Hyperintense HCCs on hepatobiliary phase gadoxetic acid–enhanced MR images show significantly lower serum level of α fetoprotein, *Lens culinaris* agglutinin reactive fraction of α fetoprotein, and protein induced by Vitamin K absence or antagonist-II than hypointense HCCs ($P = .003$, $P = .004$, and $P = .026$, respectively).
- Hyperintense HCCs on hepatobiliary phase gadoxetic acid–enhanced MR images similarly show significantly weaker expression of α fetoprotein and protein induced by Vitamin K absence or antagonist-II at immunohistochemical evaluation than did hypointense HCCs (both $P < .001$).
- Hyperintense HCCs on gadoxetic acid–enhanced MR images show a significantly lower recurrence rate than do hypointense HCCs ($P = .039$).

Implication for Patient Care

- Hypervascular HCCs that show hyperintensity on hepatobiliary phase gadoxetic acid–enhanced MR images have biologically less aggressive features than do those that show hypointensity.

Materials and Methods

Patients

This retrospective study received the approval of the institutional ethics committee, and informed consent for using the MR images and resected specimens was obtained from all patients. There were 207 consecutive patients who had 233 HCCs that were surgically resected

Published online
10.1148/radiol.12120226 **Content codes:** GI MR

Radiology 2012; 265:780–789

Abbreviations:
AFP = α-fetoprotein
HCC = hepatocellular carcinoma
L-3 = *Lens culinaris* agglutinin reactive fraction
mAU = milli–arbitrary unit
OATP = organic anion transporting polypeptide
PIVKA-II = protein induced by vitamin K absence or antagonist-II
SI = signal intensity
TR = repetition time

Author contributions:
Guarantors of integrity of entire study, A.K., O.M., K.K., S. Kobayashi, T.G., S. Kaneko, Y.N., S.A.; study concepts/study design or data acquisition or data analysis/interpretation, all authors; manuscript drafting or manuscript revision for important intellectual content, all authors; approval of final version of submitted manuscript, all authors; literature research, A.K., O.M., N.Y., K.K., S. Kobayashi, S. Kaneko, Y.N., S.A.; clinical studies, A.K., O.M., K.K., S. Kobayashi, W.K., T.G., T.Y., S. Kaneko, R.K., S.A.; experimental studies, A.K., N.Y., Y.N., S.A.; statistical analysis, A.K.; and manuscript editing, A.K., O.M., S. Kobayashi, T.G., S. Kaneko, S.A.

Conflicts of interest are listed at the end of this article.

at our institution and six affiliated institutions from April 2008 to September 2011. Patients were excluded if they had more than one HCC (12 patients with 31 nodules), if they had previous treatment (three patients with 10 nodules), if they did not have MR imaging (nine patients with nine nodules) or if their lesions were hypovascular in the arterial phase (three patients with three nodules) (Fig E1 [online]). Average age was 65.0 years ± 10.3 (range, 34–83) (age of men 64.5 years ± 10.5 [range, 34–83 years]; women, 67.4 years ± 9.5 [43–83 years]). Ratio of men to women was 138 (76.7%) to 42 (23.3%). The background liver was normal in 28 patients, whereas 70 patients had chronic hepatitis and 82 had cirrhosis. The origin of liver disease was viral hepatitis type B in 41 patients, type C in 85, types B and C in two, alcoholism in nine, and other origins in 43. Hepatic function was classified as Child-Pugh class A in 169 patients and class B in 11. Average tumor size was 33.8 mm ± 23.4 (range, 7–160 mm).

Gadoxetic Acid–enhanced MR Imaging

Gadoxetic acid–enhanced MR imaging was performed 52.8 days ± 25.3 [range, 3–95 days] before surgical resection for the characterization and pretreatment staging of HCC. MR images were obtained on several MR systems: Signa HDx 1.5 T and 3 T (GE Medical Systems, Milwaukee, Wis), Intera Achieva 1.5 T (Philips Medical Systems, Best, Netherlands), Symphony 1.5 T (Siemens, Erlangen, Germany) and Magnetom Vision 1.5 T (Siemens). MR imaging was performed with fat-suppressed two-dimensional or three-dimensional gradient-echo T1-weighted sequences (repetition time, 3.2–4.0 msec; echo time, 1.6–2.3 msec; flip angle, 10–15 degrees; field of view, 33–42 cm; matrix, 128–192 interpolated to 256–512; section thickness, 4.0–8.0 mm). For dynamic study, a dose of 0.1 mL per kilogram of 0.25 mmol/mL of gadoxetic acid (Primovist, Bayer Schering Pharma, Berlin) was injected intravenously at a flow rate of 1–2.0 mL per second, followed by a 20–40 mL saline flush. To obtain the optimal arterial dominant phase, the following methods were used. In the bolus tracking method, arterial phase timing was determined as the peak time of the abdominal aorta plus 7–15 seconds. In the test injection method (1.5 mL of Primovist + 8 mL saline flush), arterial-phase timing was determined as the peak time of the abdominal aorta plus 10 seconds minus half of imaging time. Portal phase and equilibrium phase images were obtained at 60–90 seconds and 120–180 seconds after injection, respectively. The hepatobiliary phase images were obtained 15–20 minutes after the injection.

Analysis of SI on Gadoxetic Acid–enhanced MR Images

Image analysis was performed by two abdominal imaging radiologists (A.K. and O.M., with 10 and 40 years of experience, respectively) without information on clinical and pathologic results. The SI of the tumor and surrounding background liver was individually measured and then averaged by placing regions of interest during the hepatobiliary phase. The region of interest of the tumor was determined as the maximum oval or round area at the level of the largest diameter of the tumor, avoiding degeneration area and artifact. The average size of the region of interest was 923.6 mm^2 ± 1418.3 (range, 61–6167 mm^2). The average intensity of the entire region of interest was used for analysis. A region of interest of the same size as the tumors was placed on the adjacent liver parenchyma, avoiding the large vessels.

Hypointense HCC was defined as showing lower SI than that of the surrounding liver (tumor SI/background SI < 1.0) (Fig 1a), and hyperintense HCC as showing equal or higher SI (tumor SI/background SI ≥ 1.0) (Fig 2a).

The Enhancement Ratio in the Hepatobiliary Phase

To evaluate the uptake level of gadoxetic acid, we calculated the enhancement ratio of HCCs in the hepatobiliary phase. We could not consistently assess all patients because they were examined with various MR systems and by using somewhat different parameters. As a result, we focused on only 79 HCCs studied at our institution because they were imaged by a variable flip angle method for measuring T1 value. MR images were obtained with either a 1.5-T or 3-T MR system (Signa HDx; GE Medical Systems, Milwaukee, Wis). MR imaging was performed with fat-suppressed three-dimentional spoiled gradient-echo in the steady state T1-weighted sequences (liver acquisition with volume acceleration; generalized encoding matrix; repetition time, 3.2–4.0 msec; echo time, 1.6 msec; flip angle, 6–15 degrees; field of view, 42 × 42 cm; matrix, 192 × 320, interpolated to 512 × 512; section thickness, 4.2 mm; overlap, 2.1 mm). The unenhanced phase was imaged with two different flip angles to calculate the static T1 value. The hepatobiliary phase images were obtained 20 minutes after the injection. The static T1 value before enhancement ($T1_{pre}$) was calculated as follows:

$$\exp(-TR/T1_{pre}) = (SI_A \sin\beta - S_B \sin\alpha)/(SI_A \sin\beta \cos\alpha - SI_B \sin\alpha \cos\beta)$$

where TR is repetition time and SI_A and SI_B represent the signal intensity in flip angle α and β, respectively. The enhanced images were obtained with the same parameters by using flip angle α. Then the T1 value after enhancement ($T1_{post}$) was calculated as follows:

$$\exp(-TR/T1_{post}) = \{SI_{pre}[1-\exp(-TR/T1_{pre})\cos\alpha] + SI_{post}[\exp(-TR/T1_{pre})-1]\} / \{SI_{pre}[1-\exp(-TR/T1_{pre})\cos\alpha] + SI_{post}[\exp(-TR/T1_{pre})-1]\cos\alpha\}$$

The enhancement ratio was shown as (8)

$$(1/T1_{post} - 1/T1_{pre})/(1/T1_{pre})$$

Histologic Diagnosis

Hematoxylin and eosin staining was carried out in tissue sections of all 180

Figure 1

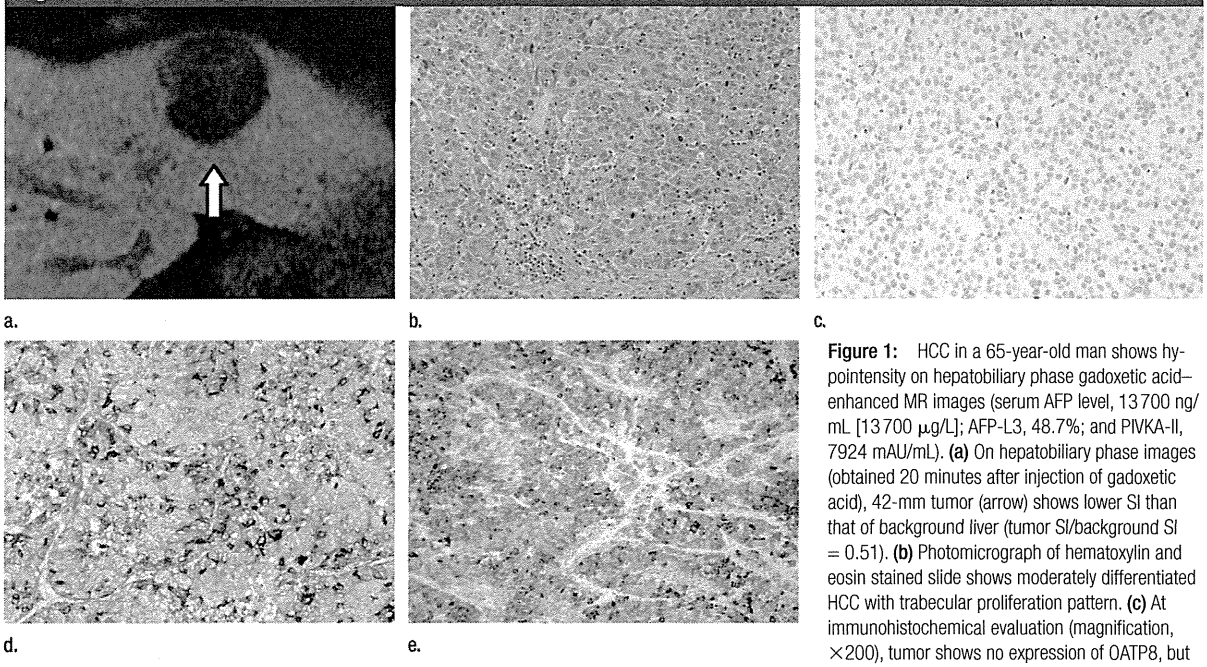

Figure 1: HCC in a 65-year-old man shows hypointensity on hepatobiliary phase gadoxetic acid–enhanced MR images (serum AFP level, 13700 ng/mL [13700 μg/L]; AFP-L3, 48.7%; and PIVKA-II, 7924 mAU/mL). **(a)** On hepatobiliary phase images (obtained 20 minutes after injection of gadoxetic acid), 42-mm tumor (arrow) shows lower SI than that of background liver (tumor SI/background SI = 0.51). **(b)** Photomicrograph of hematoxylin and eosin stained slide shows moderately differentiated HCC with trabecular proliferation pattern. **(c)** At immunohistochemical evaluation (magnification, ×200), tumor shows no expression of OATP8, but **(d)** intense expression of both AFP (brown color) and **(e)** PIVKA-II (brown color).

liver specimens. HCCs were diagnosed by consensus of two liver pathologists (S.K and Y.N. with 10 and 38 years of experience, respectively), according to the classification proposed by the International Working Party (14) and the World Health Organization classification (15). We compared hypointense HCCs and hyperintense HCCs with regard to histologic features such as macroscopic growth patterns (indistinct margin, simple nodular, extranodular growth, and multinodular patterns) (16), differentiation grade (well, moderately, and poorly differentiated), proliferation pattern (trabecular, pseudoglandular, scirrhous, and compact pattern), fibrous capsule invasion, portal vein invasion and hepatic vein invasion.

Measuring Serum Levels of AFP and PIVKA-II

Preoperative patient serum levels were obtained 10.2 days ± 7.3 (range, 0–35 days) before or after MR imaging. Serum AFP levels were measured by using chemiluminescent enzyme immunoassay (Lumipulse presto; Fujirebio, Tokyo, Japan). Serum AFP-L3 levels were measured by means of liquid-phase binding assay-electrokinetic analyte transport assay (LBA AFP-L3; Wako Pure Chemical Industries, Osaka, Japan), and were expressed as the ratio of AFP-L3 to total AFP percentage. Serum PIVKA-II levels were measured by electrochemiluminescence immunoassay (Picolumi PIVKA-II; Eidia, Tokyo, Japan) and were expressed in milli-arbitrary units (mAUs).

Immunohistochemical Analysis of AFP, PIVKA-II, and OATP8

Immunostaining was performed for all HCC specimens by using the primary antibodies human AFP (rabbit polyclonal; DAKO, Glostrup, Denmark), human PIVKA-II (MU-3 mouse monoclonal; Eidia, Tokyo, Japan) and human OATP8 (mouse monoclonal NB100-74482; Novus Biologicals, Littleton, Colo).

Two abdominal imaging radiologists (N.Y. and A.K., with 9 and 10 years of experience, respectively, in radiology and pathologic research) independently and blindly evaluated the intensity of the AFP and PIVKA-II expression on tumor cytoplasm as follows: grade 0, no expression; grade 1, weak expression; grade 2, moderate expression; and grade 3, strong expression. Similarly, they semiquantitatively evaluated the intensity of OATP8 expression on tumor cellular membranes compared with the background hepatocytes as follows: grade 0, no expression; grade 1, decreased expression; grade 2, equivalent expression; and grade 3, increased expression. We analyzed the average grades of the two investigators.

Then, we compared hypointense and hyperintense HCCs for clinical and histologic features and AFP/PIVKA-II expression (serum level and immunohistochemical analysis). To examine whether the AFP and PIVKA level simply correlates with the differentiation grade of HCCs, we performed the same analysis excluding 42 poorly differentiated HCCs. We analyzed the correlation

Figure 2

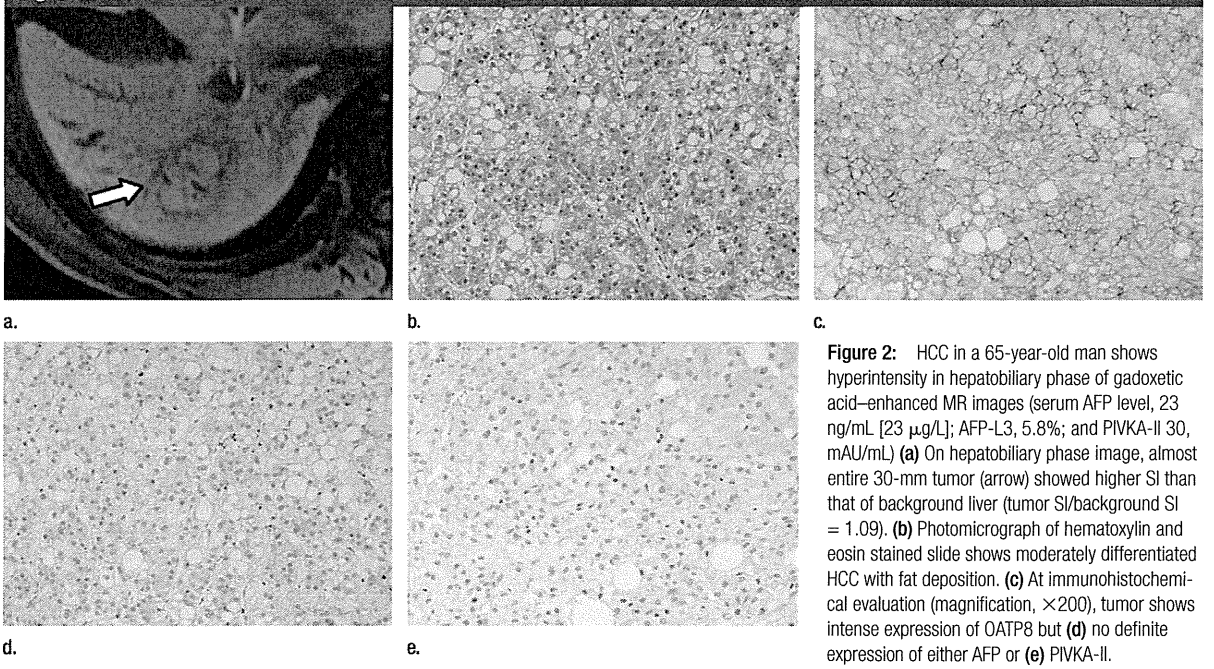

Figure 2: HCC in a 65-year-old man shows hyperintensity in hepatobiliary phase of gadoxetic acid–enhanced MR images (serum AFP level, 23 ng/mL [23 μg/L]; AFP-L3, 5.8%; and PIVKA-II 30, mAU/mL) **(a)** On hepatobiliary phase image, almost entire 30-mm tumor (arrow) showed higher SI than that of background liver (tumor SI/background SI = 1.09). **(b)** Photomicrograph of hematoxylin and eosin stained slide shows moderately differentiated HCC with fat deposition. **(c)** At immunohistochemical evaluation (magnification, ×200), tumor shows intense expression of OATP8 but **(d)** no definite expression of either AFP or **(e)** PIVKA-II.

among the immunohistochemical AFP, PIVKA-II, and OATP8 expression. We also analyzed the correlation among enhancement ratio and serum levels and immunohistochemical AFP and PIVKA-II expression for 79 HCCs.

Recurrence and Survival Rates in Patients with HCC

We compared the two groups for recurrence (including all local recurrence and intrahepatic and extrahepatic metastasis) and survival duration from the operation day. The follow-up length was 727 days ± 365 (range, 22–1293 days). When intrahepatic hypervascular HCCs or obvious extrahepatic metastasis appeared on follow-up dynamic computed tomography or gadoxetic acid–enhanced MR imaging, we considered it to be recurrence.

Statistical Analyses

Statistical significance was evaluated with GraphPad Prism5 (GraphPad Software, San Diego, Calif) and Excel Statistics 2010 (Social Survey Research Information, Tokyo, Japan). We used the Fisher test for the analysis of the clinical and histologic features; Mann-Whitney test for the comparison of serum and immunohistochemical tumor marker levels; Pearson correlation test for the correlations among AFP, PIVKA-II, OATP8 expression and enhancement ratio; and κ test for the evaluation of interobserver variation in the analysis of immunohistochemistry. The κ test score (the level of agreement) was defined as follows: 0.0–0.40, poor; 0.41–0.60, moderate; 0.61–0.80, good to fair; and 0.81–1.0, excellent. Kaplan-Meier analysis with Log-rank test, logistic regression, and Cox regression were performed for the evaluation of clinical outcome and recurrence. A P value less than 0.05 was considered to indicate a statistically significant difference.

Results

Clinical Features of the Two Types of HCC

One hundred and fifty-eight nodules were classified as hypointense HCCs (average tumor SI/background SI, 0.46 ± 0.11; range, 0.24–0.67) and the remaining 22 nodules were classified as hyperintense HCC (average tumor SI/background SI, 1.19 ± 0.22; range, 1.06–1.86). No significant differences were observed in clinical features such as sex, background liver, liver function, or tumor size between the patients with hypointense HCC and hyperintense HCC, but there was a significant difference for age (Table 1). The patients with hyperintense HCCs were significantly older than those with hypointense HCCs (P = .04).

Pathologic Features of the Two Types of HCC

None of the differences noted in the macroscopic growth patterns between the hypointense and hyperintense HCCs were significant (P = .77) (Fig E2a [online]). The hyperintense HCCs showed significantly higher differentiation grade than the hypointense HCCs (P = .028) (Fig E2b [online]). Pseudoglandular pattern was more frequently seen in hyperintense HCCs than in hypointense HCCs (Fig E2c [online]). There was a significant difference in the proliferation

Table 1

Clinical Features of Patients

Clinical Features	Hypointense HCCs	Hyperintense HCCs	*P* Value
No. of tumors	158	22	
Resected tumor size (mm)	33.2 ± 22.9 (7–160)*	37.7 ± 18.9 (10–105)*	.38
Age (y)	64.6 ± 10.3 (34–83)*	69.5 ± 7.8 (52–81)*	.04
Sex			.30
Men	119	3	
Women	39	19	
Background liver tissue			.23
Normal liver	23	5	
Chronic hepatitis	65	5	
Liver cirrhosis	70	12	
Origin of liver disease			.10
Hepatitis B	38	3	
Hepatitis C	74	11	
Hepatitis B and C	2	0	
Alcoholism	6	3	
Other	38	5	
Child Pugh classification			.63
A	149	20	
B	9	2	

Note.—Unless otherwise indicated, data are number of patients.

* Data are means ± standard deviations, with ranges in parentheses.

pattern between the hypointense and hyperintense HCCs ($P < .001$). The hypointense HCCs showed higher positive rates for fibrous capsule invasion and hepatic vein invasion, although the differences did not reach statistical significance ($P = .81$ and .21, respectively). The hyperintense HCCs showed a significantly lower rate of portal vein invasion than that of hypointense HCCs ($P = .039$) (Fig E2e [online]).

Serum Levels of AFP, AFP-L3 Fraction, and PIVKA-II

The serum levels of tumor markers AFP, AFP-L3, and PIVKA-II were significantly lower in the patients with hyperintense HCCs than in those with hypointense HCCs ($P = .003$, .004, and .026) (Figs 3, E3 [online]). To examine whether the AFP and PIVKA levels correlated with the differentiation grade of the HCCs, we performed the same analysis, excluding 42 poorly differentiated HCCs (Fig E4 [online]). Despite excluding poorly differentiated HCCs, the serum levels of these markers were also lower in the patients with hyperintense HCCs than in those with hypointense HCCs ($P = .005$, .019, and .08).

Immunohistochemistry of AFP and PIVKA-II in HCCs

In the semiquantitative analyses of immunohistochemical OATP8, AFP, and PIVKA-II, interobserver agreement of the two readers was good to excellent ($\kappa = 0.82$, 0.78, and 0.81, respectively). In immunohistochemical analysis, OATP8 expression was significantly decreased in hypointense HCCs compared with that in hyperintense HCCs ($P < .001$) (Fig 4a). The AFP expression was significantly higher in hypointense HCCs than that in hyperintense HCCs ($P < .001$) (Fig 4b). There was a significant negative correlation between AFP expression and OATP8 expression ($P = .002$, $R = -0.22$) (Fig E5c [online]). The immunohistochemical PIVKA-II expression was also significantly higher in hypointense HCCs than that in hyperintense HCCs ($P < .001$) (Fig 4c). There was a significant negative correlation between PIVKA-II expression and OATP8 expression ($P < .001$, $R = -0.38$) (Fig E5e [online]). We also performed the same immunohistochemical analysis excluding poorly differentiated HCCs (Fig E6 [online]). The expression of OATP8 was significantly lower, but expression of AFP and PIVKA-II was significantly higher in hypointense HCCs than those in hyperintense HCCs (both $P < .001$). There was still a significant negative correlation between AFP and OATP8 expression ($P = .0017$, $R = -0.27$) and between PIVKA-II and OATP8 expression ($P < .001$, $R = -0.46$).

Relative Enhancement Ratio on Hepatobiliary Phase and AFP or PIVKA-II Production

We analyzed the correlation between relative enhancement ratio and tumor marker expression for 79 HCCs (69 hypointense and 10 hyperintense HCCs). Significant negative correlations were noted among the enhancement ratio and serum AFP ($P = .023$, $R = -0.25$), serum AFP-L3 ($P < .001$, $R = -0.49$) and serum PIVKA-II level ($P = .018$, $R = -0.26$) (Fig E7a, E7b [online]). At immunohistochemical analysis, we also confirmed significant negative correlations among the enhancement ratio and AFP expression ($P = .007$, $R = -0.30$) and PIVKA-II expression ($P = .009$, $R = -0.29$) (Fig E7d, E7e [online]).

Analysis of Prognosis in Patients with HCC

The patients with hyperintense HCCs showed a significantly lower recurrence rate than those with hypointense HCCs ($P = .039$). The patients with hyperintense HCCs tended to show longer survival than those with hypointense HCCs, although without significant difference ($P = .07$) (Fig 5). Clinical features such as age and tumor size did not affect the recurrence and survival curves (Table E1 [online]). The summary of results is shown in Table 2.

Discussion

In our study, hyperintense HCCs in the hepatobiliary phase showed sig

Figure 3

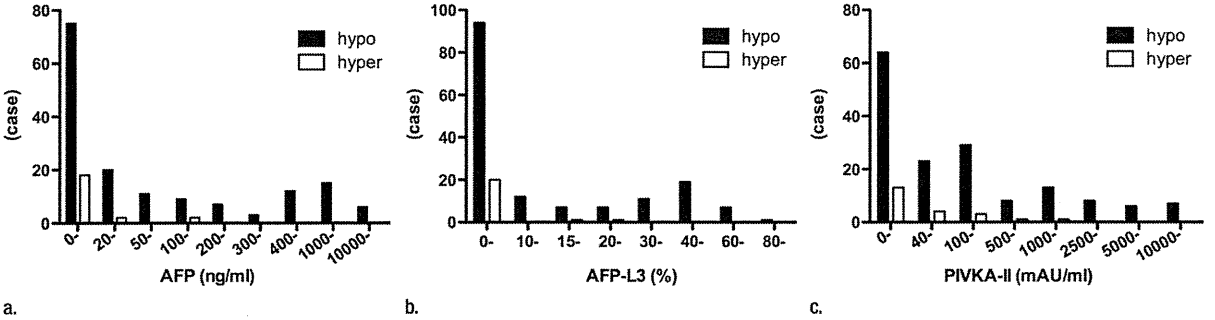

Figure 3: Graphs show serum levels of AFP, AFP-L3, and PIVKA-II. **(a)** Serum level of AFP was in normal range (<20 ng/mL [<20 μg/L]) in 18 of 22 patients (82%) with hyperintense HCCs and in 75 of 158 (47%) of patients with hypointense HCCs. Average serum AFP value was 1202.7 ng/mL ± 4369.9 [1202.7 μg/L ± 4369.9] in patients with hypointense HCCs and 17.9 ng/mL ± 29.0 [17.9 μg/L ± 29.0] in patients with hyperintense HCC, ($P = .003$). **(b)** Serum level of AFP-L3 was in normal range (<10%) in 20 of 22 patients (91%) with hyperintense HCCs, and 94 of 158 (59%) patients with hypointense HCCs. Average serum AFP-L3 fraction value was significantly lower in patients with hyperintense HCC (3.8% ± 7.5) than in those with hypointense HCC (15.9% ± 21.2) ($P = .004$). **(c)** Serum level of PIVKA-II was in normal range (<40 mAU/mL) in 13 of 22 (59%) patients with hyperintense HCCs, and 64 of 158 (40%) patients with hypointense HCCs. The serum level of PIVKA-II was also lower in patients with hyperintense HCCs (190.6 mAU/mL ± 468.6) than those with hypointense HCCs (1697.9 mAU/mL ± 6232.0) ($P = .026$).

Figure 4

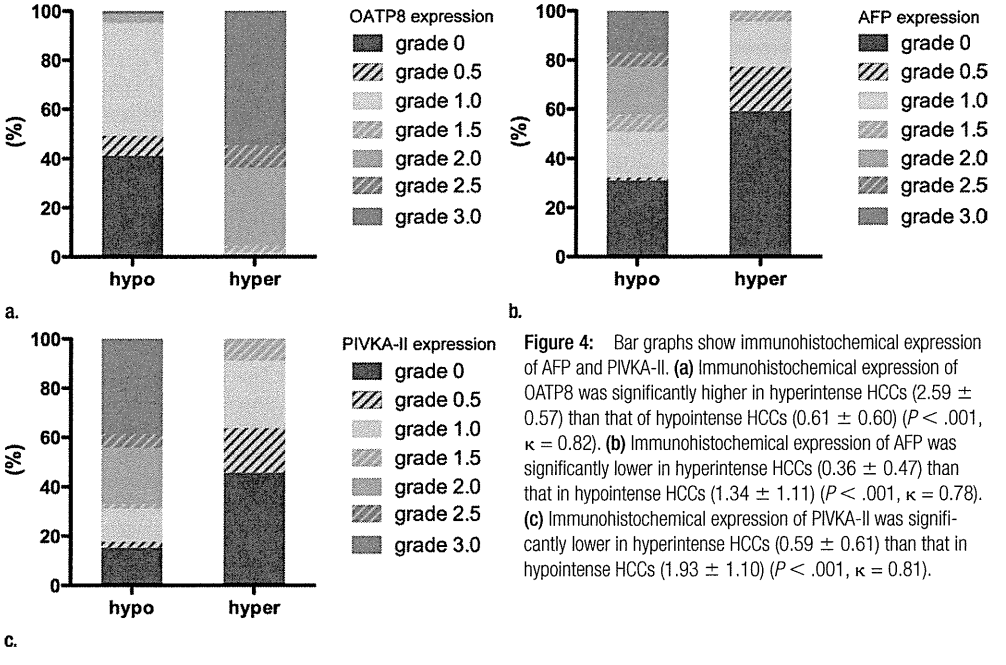

Figure 4: Bar graphs show immunohistochemical expression of AFP and PIVKA-II. **(a)** Immunohistochemical expression of OATP8 was significantly higher in hyperintense HCCs (2.59 ± 0.57) than that of hypointense HCCs (0.61 ± 0.60) ($P < .001$, $\kappa = 0.82$). **(b)** Immunohistochemical expression of AFP was significantly lower in hyperintense HCCs (0.36 ± 0.47) than that in hypointense HCCs (1.34 ± 1.11) ($P < .001$, $\kappa = 0.78$). **(c)** Immunohistochemical expression of PIVKA-II was significantly lower in hyperintense HCCs (0.59 ± 0.61) than that in hypointense HCCs (1.93 ± 1.10) ($P < .001$, $\kappa = 0.81$).

nificantly higher differentiation grades with lower frequency of portal vein invasion than did the hypointense HCCs. Moreover, hyperintense HCCs showed significantly lower expression of AFP and PIVKA-II than did hypointense HCCs. AFP and PIVKA-II levels correlated with the histologic grade of malignancy and poor prognosis (11); however, we demonstrated that the difference in tumor marker production between hypointense HCCs and hyperintense HCCs did not depend on the differentiation grade when poorly differentiated HCCs were excluded

Figure 5

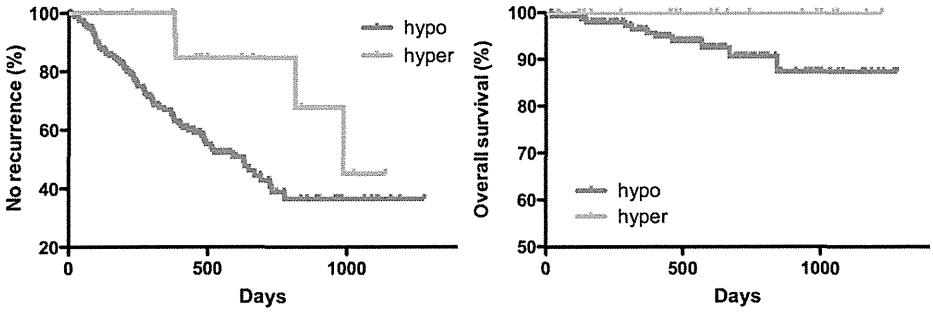

Figure 5: Charts show prognosis of patients with HCC. **(a)** Patients with hyperintense HCCs showed significantly lower recurrence rate (6 of 22, 27.2%) than did those with hypointense HCCs (83 of 158, 52.5%) ($P = .039$). **(b)** Patients with hyperintense HCCs tended to show longer survival (mortality, 0 of 22, 0%) than those with hypointense HCCs (22 of 158, 13.9%). However, there was no significant difference between the two groups ($P = .07$).

Table 2

Summary of Results

Result	Hypointense HCCs ($n = 158$)	Hyperintense HCCs ($n = 22$)	*P* Value
Macro growth pattern			.77
Indistinct margin	6	0	
Simple nodular	102	17	
Extranodular	30	3	
Multinodular	20	2	
Differentiation			.028
Well differentiated	22	4	
Moderately differentiated	94	18	
Poorly differentiated	42	0	
Proliferation pattern			<.001
Trabecular	116	12	
Pseudoglandular	20	10	
Schirrous	9	0	
Compact	13	0	
Fibrous capsule invasion	63 (39.9%)	8 (36.4%)	.810
Portal vein invasion	58 (36.7%)	3 (13.6%)	.039
Hepatic vein invasion	21 (13.3%)	0 (0%)	.210
Serum levels			
AFP (ng/mL)	1202.7 ± 4369.9 (497.4 ± 1899.1*)	17.9 ± 29.0	.003 (.005*)
AFP-L3 (%)	15.9 ± 21.2 (14.5 ± 21.0*)	3.8 ± 7.5	.004 (.019*)
PIVKA-II (mAU/mL)	1697.9 ± 6232.0 (1497.6 ± 7067.9*)	190.6 ± 468.6	.026 (.08*)
Immunohistochemical analysis			
OATP8	0.61 ± 0.60 (0.67 ± 0.63*)	2.59 ± 0.57	<.001 (<.001*)
AFP	1.34 ± 1.11 (1.34 ± 1.10*)	0.36 ± 0.47	<.001 (<.001*)
PIVKA-II	1.93 ± 1.10 (1.87 ± 1.08*)	0.59 ± 0.61	<.001 (<.001*)
Recurrence rate	83 (52.5%)	6 (27.2%)	.039
Survival rate	22 (86.1%)	22 (100%)	.070

* Excluding poorly differentiated HCCs ($n = 42$).

from the analysis. We suspect that the molecular regulatory mechanism of OATP8 expression may have some common channels with those of AFP or PIVKA-II expression.

In addition, hyperintense HCCs on hepatobiliary phase images showed a significantly lower recurrence rate than did hypointense HCCs. The patients with hyperintense HCCs showed longer survival than those with hypointense HCCs, but the difference was not statistically significant. In our study, the follow-up period averaged 727 days, which might not have been sufficient to demonstrate a significant difference.

Several prior reports have suggested that transcription factor hepatocyte nuclear factors control both OATP8 and AFP expression (9,12,13,17). Therefore, we speculated that some correlation between OATP8 and AFP expression through the hepatocyte nuclear factor family might exist. The regulatory mechanism of PIVKA-II and the correlation with OATP8 expression in HCC have not yet been determined. The transcription of the OATP8 gene is also regulated by the nuclear factor (steroid and xenobiotics receptor or pregnane xenobiotics receptor) (18). Vitamin K can be the ligand of these receptors, and it regulates the transcription of target genes (19). If vitamin

K decreases in HCC, the PIVKA-II production increases (20). We suspected that the transcription of OATP8 might change in accordance with the decrease of ligands to these receptors. As a result, we expected that PIVKA-II expression and OATP8 expression might be correlated.

However, there were many patients that showed low AFP and PIVKA-II expression in hypointense HCCs. We attribute this to the fact that OATP8, AFP, and PIVKA-II have several direct and indirect regulatory mechanisms other than the hepatocyte nuclear factor route (21). Further investigation is needed to clarify the real underlying molecular biology of these correlations.

The molecular classification of subtypes of HCCs is now being investigated by several groups (22). Yamashita et al (23,24) reported on HCC subtypes that were classified on the basis of expression of AFP and epithelial cell adhesion molecule, a stem cell marker. According to their reports, AFP-positive and epithelial cell adhesion molecule–positive HCCs showed stem and progenitor cell features with invasive character and poor prognosis compared with AFP-negative and epithelial cell adhesion molecule–negative HCCs that demonstrated mature hepatocyte-like features with a relatively good prognosis. These features of AFP-negative and epithelial cell adhesion molecule–negative HCCs resembled those of hyperintense HCCs, and we surmised that the origin of hyperintense HCC may be mature hepatocyte-like cells rather than stem or progenitor cells. We think that hyperintense HCCs may have some specific molecular or genetic profiles. Further molecular and genetic analyses are needed to clarify the exact molecular biologic basis for this possible subtype of HCCs.

Our study had limitations. First, the total number of hyperintense HCCs examined was small because such tumors are relatively rare (8). Second, we only assessed HCC lesions that were hypervascular in the arterial phase, and therefore our results cannot be applied to a general screening population with benign disease, hypovascular HCC on arterial-phase images, or other malignancies. Third, there was a variability of the imaging parameters, such as strength of magnetic field, section thickness, and on imaging timing, because this was multicenter study.

In conclusion, hyperintense HCCs on hepatobiliary phase images showed significantly higher differentiation grades, less frequent portal vein invasion, and lower recurrence rates than did hypointense HCCs. Moreover, hyperintense HCCs showed significantly lower expression of AFP and PIVKA-II than did hypointense HCCs. Hyperintense HCCs on hepatobiliary phase gadoxetic acid–enhanced MR images may be a particular form of hypervascular HCC with biologically less aggressive features than those of hypointense HCCs.

Acknowledgments: We deeply appreciate Dr. Taro Yamashita (Department of Gastroenterology, Kanazawa University Graduate School of Medical Science, Kanazawa, Japan), Dr. Yoh Zen (Institute of Liver Studies, King's College Hospital, London, United Kingdom) and Dr. Seiko Kitamura-Sawada (Division of Pathology, Kanazawa University Hospital, Kanazawa, Japan) for their support to our study.

Disclosures of Conflicts of Interest: A.K. No relevant conflicts of interest to disclose. **O.M.** Financial activities related to the present article: Received a consulting fee or honorarium and fees for participation in review activities from Bayer Japan. Financial activities not related to the present article: none to disclose. Other relationships: none to disclose. **N.Y.** No relevant conflicts of interest to disclose. **K.K.** No relevant conflicts of interest to disclose. **S.Kobayashi.** No relevant conflicts of interest to disclose. **W.K.** No relevant conflicts of interest to disclose. **T.G.** No relevant conflicts of interest to disclose. **T.Y.** No relevant conflicts of interest to disclose. **S.Kaneko.** No relevant conflicts of interest to disclose. **Y.N.** No relevant conflicts of interest to disclose. **R.K.** No relevant conflicts of interest to disclose. **S.A.** No relevant conflicts of interest to disclose.

References

1. Caldwell S, Park SH. The epidemiology of hepatocellular cancer: from the perspectives of public health problem to tumor biology. J Gastroenterol 2009;44(Suppl 19):96–101.
2. Ahn SS, Kim MJ, Lim JS, Hong HS, Chung YE, Choi JY. Added value of gadoxetic acid-enhanced hepatobiliary phase MR imaging in the diagnosis of hepatocellular carcinoma. Radiology 2010;255(2):459–466.
3. Ichikawa T, Saito K, Yoshioka N, et al. Detection and characterization of focal liver lesions: a Japanese phase III, multicenter comparison between gadoxetic acid disodium-enhanced magnetic resonance imaging and contrast-enhanced computed tomography predominantly in patients with hepatocellular carcinoma and chronic liver disease. Invest Radiol 2010;45(3):133–141.
4. Golfieri R, Renzulli M, Lucidi V, Corcioni B, Trevisani F, Bolondi L. Contribution of the hepatobiliary phase of Gd-EOB-DTPA-enhanced MRI to Dynamic MRI in the detection of hypovascular small (≤ 2 cm) HCC in cirrhosis. Eur Radiol 2011;21(6):1233–1242.
5. Kitao A, Zen Y, Matsui O, et al. Hepatocellular carcinoma: signal intensity at gadoxetic acid-enhanced MR Imaging—correlation with molecular transporters and histopathologic features. Radiology 2010;256(3):817–826.
6. Narita M, Hatano E, Arizono S, et al. Expression of OATP1B3 determines uptake of Gd-EOB-DTPA in hepatocellular carcinoma. J Gastroenterol 2009;44(7):793–798.
7. Asayama Y, Tajima T, Nishie A, et al. Uptake of Gd-EOB-DTPA by hepatocellular carcinoma: radiologic-pathologic correlation with special reference to bile production. Eur J Radiol 2011;80(3):e243–e248.
8. Kitao A, Matsui O, Yoneda N, et al. The uptake transporter OATP8 expression decreases during multistep hepatocarcinogenesis: correlation with gadoxetic acid enhanced MR imaging. Eur Radiol 2011;21(10):2056–2066.
9. Jung D, Hagenbuch B, Gresh L, Pontoglio M, Meier PJ, Kullak-Ublick GA. Characterization of the human OATP-C (SLC21A6) gene promoter and regulation of liver-specific OATP genes by hepatocyte nuclear factor 1 alpha. J Biol Chem 2001;276(40):37206–37214.
10. Inagaki Y, Tang W, Xu H, et al. Des-gamma-carboxyprothrombin: clinical effectiveness and biochemical importance. Biosci Trends 2008;2(2):53–60.
11. Miyaaki H, Nakashima O, Kurogi M, Eguchi K, Kojiro M. Lens culinaris agglutinin-reactive alpha-fetoprotein and protein induced by vitamin K absence II are potential indicators of a poor prognosis: a histopathological study of surgically resected hepatocellular carcinoma. J Gastroenterol 2007;42(12):962–968.
12. Nakabayashi H, Koyama Y, Suzuki H, et al. Functional mapping of tissue-specific elements of the human alpha-fetoprotein gene enhancer. Biochem Biophys Res Commun 2004;318(3):773–785.

13. Ishii K, Yoshida Y, Akechi Y, et al. Hepatic differentiation of human bone marrow-derived mesenchymal stem cells by tetracycline-regulated hepatocyte nuclear factor 3beta. Hepatology 2008;48(2):597–606.

14. Hirohashi S, Ishak KG, Kojiro M, et al. Hepatocellular carcinoma. In: Hamilton SR, Aaltonen LA, eds. Pathology and genetics of tumours of the digestive system. Lyon, France: IARC, 2000; 157–172.

15. International Consensus Group for Hepatocellular Neoplasia. Pathologic diagnosis of early hepatocellular carcinoma: a report of the international consensus group for hepatocellular neoplasia. Hepatology 2009;49(2):658–664.

16. Liver Cancer Study Group of Japan. General rules for the clinical and pathological study of primary liver cancer. 3rd ed. Tokyo, Japan: Kanehara, 2010.

17. Vavricka SR, Jung D, Fried M, Grützner U, Meier PJ, Kullak-Ublick GA. The human organic anion transporting polypeptide 8 (SLCO1B3) gene is transcriptionally repressed by hepatocyte nuclear factor 3beta in hepatocellular carcinoma. J Hepatol 2004;40(2):212–218.

18. Gui C, Miao Y, Thompson L, et al. Effect of pregnane X receptor ligands on transport mediated by human OATP1B1 and OATP1B3. Eur J Pharmacol 2008;584(1):57–65.

19. Azuma K, Urano T, Ouchi Y, Inoue S. Vitamin K2 suppresses proliferation and motility of hepatocellular carcinoma cells by activating steroid and xenobiotic receptor. Endocr J 2009;56(7):843–849.

20. Huisse MG, Leclercq M, Belghiti J, et al. Mechanism of the abnormal vitamin K-dependent gamma-carboxylation process in human hepatocellular carcinomas. Cancer 1994;74(5):1533–1541.

21. Saito S, Ojima H, Ichikawa H, Hirohashi S, Kondo T. Molecular background of alpha-fetoprotein in liver cancer cells as revealed by global RNA expression analysis. Cancer Sci 2008;99(12):2402–2409.

22. Lee JS, Heo J, Libbrecht L, et al. A novel prognostic subtype of human hepatocellular carcinoma derived from hepatic progenitor cells. Nat Med 2006;12(4):410–416.

23. Yamashita T, Ji J, Budhu A, et al. EpCAM-positive hepatocellular carcinoma cells are tumor-initiating cells with stem/progenitor cell features. Gastroenterology 2009;136(3):1012–1024.

24. Yamashita T, Forgues M, Wang W, et al. EpCAM and alpha-fetoprotein expression defines novel prognostic subtypes of hepatocellular carcinoma. Cancer Res 2008;68(5):1451–1461.

HEPATOLOGY
Official Journal of the American Association for the Study of Liver Diseases

Transcriptomic Profiling Reveals Hepatic Stem-Like Gene Signatures and Interplay of miR-200c and Epithelial-Mesenchymal Transition in Intrahepatic Cholangiocarcinoma

Naoki Oishi,[1] Mia R. Kumar,[1] Stephanie Roessler,[1] Junfang Ji,[1] Marshonna Forgues,[1] Anuradha Budhu,[1] Xuelian Zhao,[1] Jesper B. Andersen,[2] Qing-Hai Ye,[3] Hu-Liang Jia,[3] Lun-Xiu Qin,[3] Taro Yamashita,[4] Hyun Goo Woo,[5] Yoon Jun Kim,[6] Shuichi Kaneko,[4] Zhao-You Tang,[3] Snorri S. Thorgeirsson,[2] and Xin Wei Wang[1]

Intrahepatic cholangiocellular carcinoma (ICC) is the second most common type of primary liver cancer. However, its tumor heterogeneity and molecular characteristics are largely unknown. In this study, we conducted transcriptomic profiling of 23 ICC and combined hepatocellular cholangiocarcinoma tumor specimens from Asian patients using Affymetrix messenger RNA (mRNA) and NanoString microRNA microarrays to search for unique gene signatures linked to tumor subtypes and patient prognosis. We validated the signatures in an additional 68 ICC cases derived from Caucasian patients. We found that both mRNA and microRNA expression profiles could independently classify Asian ICC cases into two main subgroups, one of which shared gene expression signatures with previously identified hepatocellular carcinoma (HCC) with stem cell gene expression traits. ICC-specific gene signatures could predict survival in Asian HCC cases and independently in Caucasian ICC cases. Integrative analyses of the ICC-specific mRNA and microRNA expression profiles revealed that a common signaling pathway linking miR-200c signaling to epithelial-mesenchymal transition (EMT) was preferentially activated in ICC with stem cell gene expression traits. Inactivation of miR-200c resulted in an induction of EMT, whereas activation of miR-200c led to a reduction of EMT including a reduced cell migration and invasion in ICC cells. We also found that miR-200c and neural cell adhesion molecule 1 (NCAM1) expression were negatively correlated and their expression levels were predictive of survival in ICC samples. NCAM1, a known hepatic stem/progenitor cell marker, was experimentally demonstrated to be a direct target of miR-200c. Conclusion: Our results indicate that ICC and HCC share common stem-like molecular characteristics and poor prognosis. We suggest that the specific components of EMT may be exploited as critical biomarkers and clinically relevant therapeutic targets for an aggressive form of stem cell-like ICC. (HEPATOLOGY 2012;56:1792-1803)

Primary liver cancer (PLC) is the second most lethal cancer for men in the world.[1] Intrahepatic cholangiocellular carcinoma (ICC) is the second most common type of PLC. Although ICC is much less common than hepatocellular carcinoma (HCC), its incidence has increased drastically over the past two decades.[2,3] However, the molecular pathogenesis of ICC is largely unknown. Understanding of the tumor

Abbreviations: CHC, combined hepatocellular cholangiocarcinoma; CSC, cancer stem cell; EMT, epithelial-mesenchymal transition; FNH, focal nodular hyperplasia; GEO, gene expression omnibus; HCC, hepatocellular carcinoma; HpSC-ICC, hepatic stem cell-like ICC; ICC, intrahepatic cholangiocarcinoma; MH-ICC, mature hepatocyte-like ICC; PLC, primary liver cancer; x-HCC; extreme HCC.

From the [1]Laboratory of Human Carcinogenesis, Center for Cancer Research, National Cancer Institute, National Institutes of Health, Bethesda, MD; [2]Laboratory of Experimental Carcinogenesis, Center for Cancer Research, National Cancer Institute, National Institutes of Health, Bethesda, MD; [3]Liver Cancer Institute, Fudan University, Shanghai, China; [4]Liver Disease Center and Kanazawa University Hospital, Kanazawa University, Kanazawa, Japan; [5]Department of Physiology, Ajou University School of Medicine, Suwon, Korea; and [6]Department of Internal Medicine and Liver Research Institute, Seoul National University College of Medicine, Seoul, Korea.

Received December 22, 2011; accepted May 19, 2012.

Supported in part by the Intramural Research Program of the center for Cancer Research, the U.S. National Cancer Institute (Z01 BC 010313 and Z01 BC 010876).

Dr. Mia R. Kumar is currently affiliated with Human Genome Sciences, Rockville, MD.

biology of HCC and ICC that contributes to tumor heterogeneity is paramount in developing effective therapies to improve patient outcome.

The cellular origin of HCC and ICC has been subject to intense debate in recent years. It is thought that HCC is derived from hepatocytes, whereas ICC arises from intrahepatic biliary epithelium. However, a mixed form of HCC and ICC, also known as combined hepatocellular cholangiocarcinoma (CHC), has been described to have distinct clinicopathological features but morphological intermediates of HCC and ICC, suggesting that HCC and ICC could share the same cellular origin.[4-6] Recent studies utilizing high-resolution genomic approaches have shed light on the revelation of cellular origin of HCC and suggest that a subset of HCC contains stem cell-like features.[7-10] For example, a subset of tumor cells isolated from HCC patients are tumor-initiating cells with stem cell traits.[11-14] Moreover, HCC may share an ICC-like gene expression trait.[15] These results are consistent with the cancer stem cell (CSC) hypothesis, which suggests that most tumor cells are derived from undifferentiated cells with stem-like capabilities and that both ICC and HCC may share the same cellular origin of hepatic stem/progenitor cells.

Global messenger RNA (mRNA) and microRNA profiling approaches have been proven to be effective in identifying genes critical to HCC.[8,9,16-22] In this study, we used both mRNA and microRNA profiling approaches to determine tumor heterogeneity and molecular characteristics of ICC. We found that ICC samples consist of at least two main subtypes that share similar molecular activities, with HCC linked to stem cell-like gene expression and patient survival. Integrative genomic analyses revealed that genes and microRNAs involved in epithelial-mesenchymal transition (EMT) are altered in stem-like ICCs. Our results shed light on ICC diagnosis and may open new avenues for therapeutic interventions for targeting poor prognosis ICC patients.

Materials and Methods

Human Subjects. ICC and CHC tissues were obtained with informed consent from Asian patients who underwent curative resection between 2002 and 2003 at the Liver Cancer Institute and Zhongshan Hospital (Fudan University, Shanghai, China) and between 2008 and 2010 at the Kanazawa University Hospital (Ishikawa, Japan). Sample collection was approved by the Institutional Review Board of the corresponding institutes and recorded by the National Institutes of Health (NIH) Office of Human Subjects Research. A total of 23 ICC and CHC cases were used to build mRNA and microRNA signatures. The initial diagnosis was made based on serological test and imaging, and was confirmed histopathologically by pathologists. The characteristics of 68 Caucasian ICC patients from an independent cohort were described recently.[23]

Cell Line, Culture, and Transfection. HuCCT1 and HUH28 cell lines were used for miR-200c functional studies. These cell lines were obtained from the Japanese Collection of Research Bioresources Cell Bank and were cultured in RPMI supplemented with 10% fetal bovine serum, 100 U/mL penicillin, 0.1 mg/mL streptomycin, and 2 mmol/L L-glutamine. An immortalized human cholangiocyte-derived cell line, H69, kindly provided by Dr. Gregory Gores (Mayo Clinic), was cultured as described.[24] A luciferase reporter containing an upstream 0.9-kb fragment of pri-miR-200c was kindly provided by Dr. Li Wang (University of Utah School of Medicine).[25] A detailed description of other transfection reagents, methodologies such as cell culture, cell proliferation and apoptosis assays, luciferase assay, immunohistochemical analysis, and cell migration and invasion assays can be found in the Supporting Materials.

Microarray Processing. Total RNA was extracted from frozen tissue using Trizol (Invitrogen) according to the manufacturer's protocol. Only RNA samples with good RNA quality as confirmed with the Agilent 2100 Bioanalyzer (Agilent Technologies) were included for array study. Gene expression profiling of 23 tumor samples (16 ICC, 7 CHC), as well as seven paired noncancerous liver tissues from ICC patients and seven benign liver lesions (five focal nodular hyperplasia [FNH], two adenoma) was carried out on Affymetrix GeneChip Human Gene-ST 1.0 arrays according to the manufacturer's protocol and processed as described.[26] Affymetrix gene expression arrays obtained from different platforms were combined with the match probes package in R. Raw gene expression data were normalized using the robust multi-array average

Address reprint requests to: Dr. Xin Wei Wang, National Cancer Institute, 37 Convent Dr., Bldg. 37, Rm. 3044A, Bethesda, MD 20892. E-mail: xw3u@nih.gov

View this article online at wileyonlinelibrary.com.
DOI 10.1002/hep.25890
Potential conflict of interest: Nothing to report.
Additional Supporting Information may be found in the online version of this article.

(RMA) method and global median centering. For genes with more than one probe set, the mean gene expression was calculated. Total RNA was used for the nCounter microRNA platform. All sample preparation and hybridization was performed according to the manufacturer's instructions. All hybridization reactions were incubated at 65°C for a minimum of 12 hours. Hybridized probes were purified and counted on the nCounter Prep Station and Digital Analyzer (NanoString) following the manufacturer's instructions. For each assay a high-density scan was performed. For platform validation using synthetic oligonucleotides, NanoString nCounter microRNA raw data were normalized for lane-to-lane variation with a dilution series of six spike-in positive controls. The sum of the six positive controls for a given lane was divided by the average sum across lanes to yield a normalization factor, which was then multiplied by the raw counts in each lane to give normalized values. Raw mRNA and microRNA data are accessible through the accession numbers GSE32879 and GSE32957 at the NCBI Gene Expression Omnibus (GEO) database. Other statistical methods can be found in the Supporting Materials.

Real-Time Reverse-Transcription Polymerase Chain Reaction (RT-PCR) Analysis. Total RNA was subjected to qRT-PCR. Mature microRNAs and other mRNAs were analyzed using the TaqMan microRNA Assays and Gene Expression Assays, respectively, in accordance with manufacturer's instructions (Applied Biosystems, Foster City, CA). All RT reactions were run in a GeneAmp PCR 9700 Thermocycler (Applied Biosystems). Probes used for the analyses were as follows: ZEB1, Hs00232783_m1; ZEB2, Hs00207691_m1; VIM, Hs00185584_m1; CDH1, Hs01023894_m1; CDH2, Hs00983056_m1; MYC, Hs00905030_m1; Hsa-miR-200c, 002300; Hsa-miR-141, 000463 (Applied Biosystems). The experiments were performed in triplicate. The TaqMan gene assay for 18s and actin was used to normalize the relative abundance of mRNA. RNU6B RNA was used as a control for miR-200c.

Results

Profiling of mRNA Expression in ICC and CHC. We performed transcriptomic analyses of 30 retrospectively collected ICC and CHC clinical specimens from Chinese (n = 13) and Japanese (n = 10) patients with seven paired nontumor liver tissues from ICC patients using Affymetrix GeneChip Human Gene-ST arrays. Five FNH cases and two adenomas were also included as benign tumors of the liver. Clinical features of these ICC and CHC cases are included in Supporting Table S1. Multidimensional scaling analysis revealed that malignant tumor samples were mainly different from benign tumors and nontumor tissues, suggesting that malignant tumors have a vastly different gene expression profile (Fig. S1). To determine tumor heterogeneity, unsupervised hierarchical clustering analysis of 23 ICC and CHC samples based on all genes was conducted. The result revealed that tumor samples can be divided into two main groups, i.e., cluster-A and cluster-B (Fig. 1A). Kaplan-Meier survival analysis revealed that ICC cases in cluster-A had a shorter survival than those in cluster-B (Fig. 1B). These results suggest that gene expression and tumor biology differ significantly among different ICC tumor samples.

We previously identified two HCC subgroups, one resembling gene expression signatures of hepatic stem cells (referred to as HpSC-HCC) and the other similar to mature hepatocyte (referred to as MH-HCC). To determine if ICC subgroups have different gene expression profiles compared to HCC subgroups, we randomly selected two groups of HCC samples, each consisting of 23 age- and gender-matched HCC cases from an existing cohort of 246 HCC samples with available Affymetrix data (GEO accession number GSE14520) and compared them with 23 ICC and CHC tumors (Table S1). Unsupervised hierarchical clustering analysis revealed two main branches. All eight cluster-A ICC samples were grouped with epithelial cell adhesion molecule $(EpCAM)^+AFP^+$ HCC cases previously identified having a stem cell-like gene expression trait, whereas all eight cluster-B ICC samples were grouped with $EpCAM^-AFP^-$ HCC cases with a mature hepatocyte-like gene expression trait (Fig. S2A).[9] Similar results were obtained when ICC/CHC cases were compared to a second group of 23 randomly selected HCC cases (Fig. S2B). Seven CHC cases were split among two clusters. For the convenience of keeping track of these ICC samples, we refer to ICC cases in cluster-A as HpSC-ICC (i.e., hepatic stem cell-like ICC) and those in cluster-B as MH-ICC (i.e., mature hepatocyte-like ICC). These results indicate that both ICC and HCC are heterogeneous and their subgroups share similar gene expression profiles.

Next, we performed a class comparison analysis and identified 636 genes that are differentially expressed between eight HpSC-ICC and eight MH-ICC cases (univariate $P < 0.01$; false discovery rate [FDR] <0.2) (Table S2). We then tested whether this 636 ICC-specific gene signature could independently classify HCC

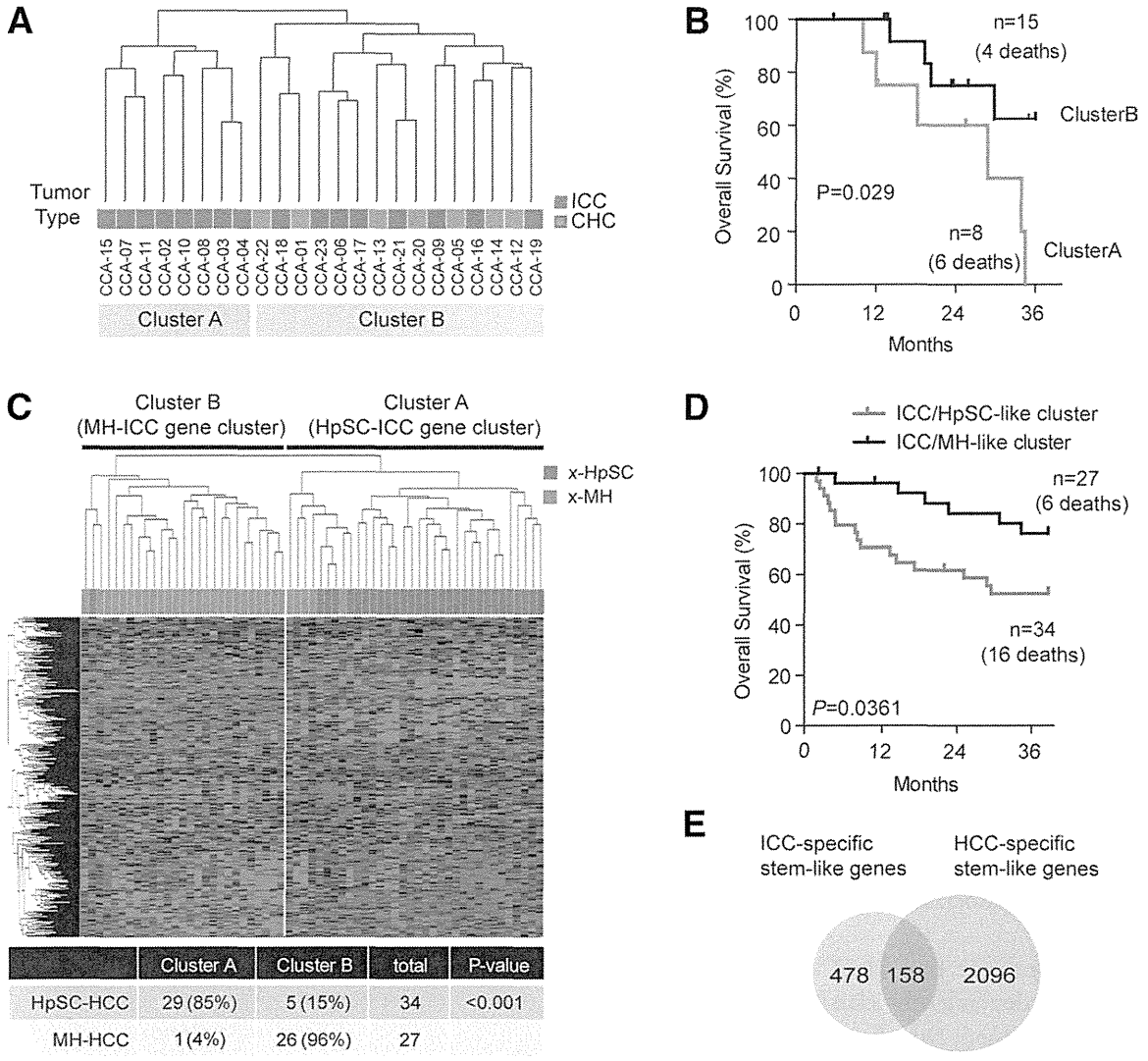

	Cluster A	Cluster B	total	P-value
HpSC-HCC	29 (85%)	5 (15%)	34	<0.001
MH-HCC	1 (4%)	26 (96%)	27	

Fig. 1. Heterogeneity of Asian ICC and HCC cases based on mRNA expression profiling. (A) Unsupervised hierarchical clustering of 23 ICC and CHC cases based on global mRNA expression using centered correlation and average linkage. The red and green bars beneath the dendrogram indicate ICC and ICC with CHC features, respectively. ICC cases in cluster-A are referred to as HpSC-ICC and ICC cases in Cluster-B are referred to as MH-ICC. (B) Kaplan-Meier analysis of ICC cases based on the classification of cluster-A and cluster-B from (A). (C) Hierarchical clustering of 61 extreme HCC cases (i.e., 34 *x*-HpSC HCC and 27 *x*-MH HCC) based on the expression of 636 ICC-specific genes. The red and green bars above the heatmap indicate *x*-HpSC and *x*-MH, respectively. A summary of HCC cases based on the dendrogram classification with the ICC-specific signature is included. A chi-squared test was used to determine the correct classification. (D) Kaplan-Meier plot of 61 extreme HCC cases based on the classification by the 636-gene signature into HpSC-ICC and MH-ICC clusters. (E) Venn-diagram of stem-like ICC genes and stem-like HCC genes.

cases based on HpSC-like or MH-like features. We tested the robustness of the signature to discriminate HpSC-HCC from MH-HCC cases by examining 61 well-defined extreme HCC cases or *x*-HCC, i.e., those with top quartile EpCAM expression in HCC tissues and with >1,000 ng/mL of serum alpha-fetoprotein (AFP) levels versus those with bottom quartile EpCAM expression and with <20 ng/mL of serum AFP levels (Table S1). Hierarchical clustering analysis revealed that the 636 ICC-specific genes could nicely divide *x*-HpSC and *x*-MH HCC cases (Fig. 1C) and were associated with HCC survival (Fig. 1D). This 636 ICC-specific gene signature was also associated with survival in 139 remaining unstratified HCC cases from the original 246 HCC cases after excluding 46 randomly selected HCC cases and 61 extreme HCC cases used in the initial clustering analysis (Fig. S2C). Venn diagram analysis indicated that 158 of 636 ICC-specific genes (25%) overlapped with previously identified stem-like HCC genes (Fig. 1E). Consistent with the data in Fig. 1C, 158 overlapping genes could significantly discriminate stem-like HCC cases from mature hepatocyte-like HCC cases ($P < 0.0001$) and was associated with HCC survival ($P = 0.031$)

(Fig. S3). The above data indicate that ICC cases could be classified into two main subtypes that are associated with stem-like or mature hepatocyte like gene expression traits, respectively, and that ICC and HCC may share common gene expression profiles reflecting their cellular origins.

Profiling of MicroRNA Expression in ICC and CHC. We used the NanoString nCounter microRNA Expression Assay platform to independently examine gene expression profiles of the same 23 ICC and CHC samples used above. Unsupervised clustering analysis based on the expression of all 700 human mature microRNAs revealed that ICCs were again divided into two main clusters, where 5 of 6 ICC cases in cluster A belong to HpSC-ICC and 7 of 10 cases in cluster-B belong to MH-ICC as assigned by mRNA expression (Fig. 2A). Class comparison analysis revealed 23 microRNAs to be differentially expressed between HpSC-ICC and MH-ICC ($P < 0.05$) (Table S3). This ICC-specific microRNA signature was further tested for its ability to classify the same HCC cohort described above with available microRNA expression data generated from an independent array platform (GEO accession number: GSE6857). Again, the ICC-specific microRNA signature could significantly discriminate well-defined extreme HCC subgroups and was associated with HCC survival (Fig. 2B,C).

Our results indicate that HpSC-ICC and MH-ICC cases can be independently classified by mRNA and microRNA expression, which suggests that these two subgroups have a clearly measurable difference at the gene expression level. We hypothesized that those HpSC-ICC tumors share the same stem-like traits with HCC with poor survival, and patients with this type of ICC would have a poor outcome. To determine if ICC-specific gene signature is predictive of ICC patient survival, we performed hierarchical clustering analysis using 158 overlapping genes (described in Fig. 1E) in 68 ICC cases from an independent cohort containing Caucasian patients (Fig. 3A). Consistently, the 158 overlapping gene signature was significantly associated with patient survival in this cohort ($P < 0.02$) (Fig. 3B). Similar results were obtained when all 636 ICC-specific genes were used for this analysis ($P < 0.04$; Fig. S4).

Integrative Pathway Analysis of ICC-Specific mRNA and MicroRNA. Because microRNA and mRNA are functionally linked, we hypothesized that the expression levels between ICC-specific mRNAs and ICC-specific microRNAs would be highly correlated, as they both are associated with the same stem

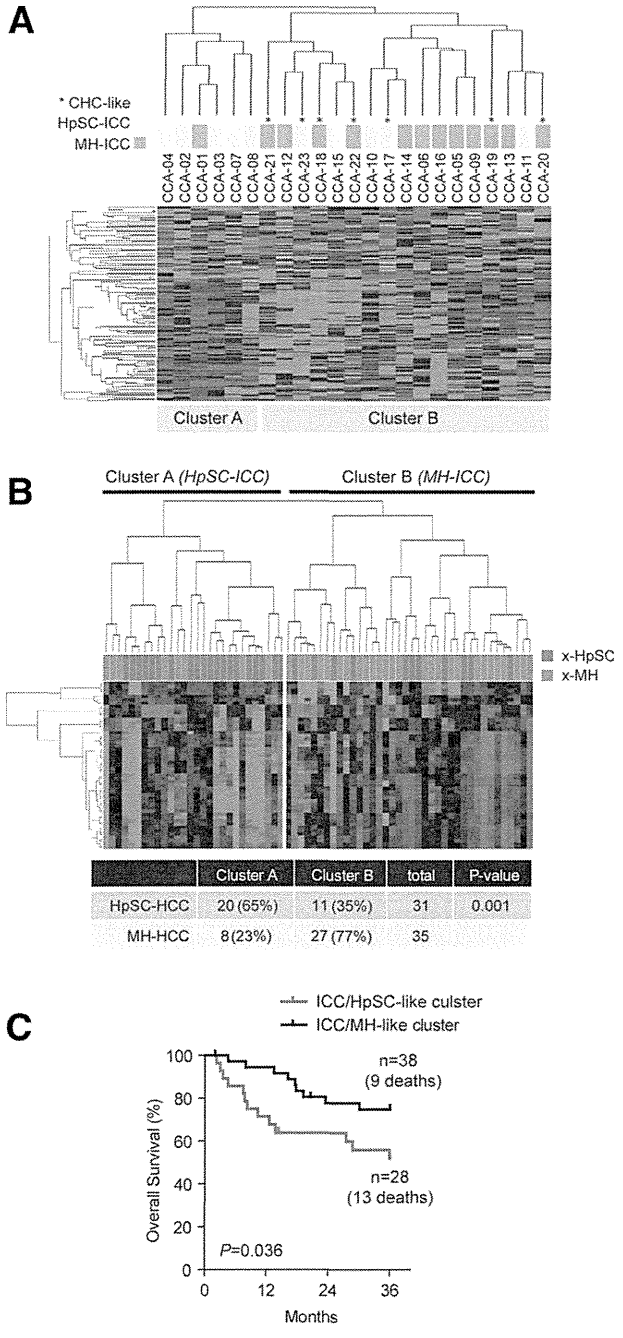

Fig. 2. Heterogeneity of Asian ICC cases revealed by microRNA expression profiling. (A) Unsupervised hierarchical clustering of 23 Asian ICC cases based on global microRNA expression using centered correlation and average linkage. The yellow and light blue bars beneath the dendrogram indicate HpSC-ICC and MH-ICC subgroups, respectively, as classified by mRNA expression profiling described in Fig. 1A. *CHC-like cases. (B) Hierarchical clustering of 61 extreme HCC cases based on the expression of 23 ICC-specific microRNAs. The red and green bars above the heatmap indicate *x*-HpSC and *x*-MH, respectively. A summary of HCC cases based on the dendrogram classification with the ICC-specific signature is included. A chi-squared test was used to determine the correct classification. (C) Kaplan-Meier plot of 61 extreme HCC cases based on the clustering results of (B).

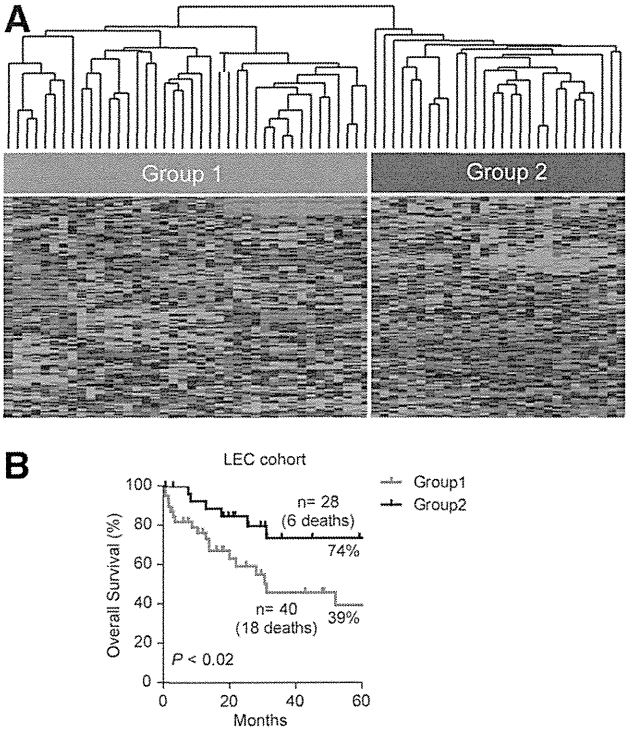

Fig. 3. Validation of the ICC-specific gene signature in an independent ICC cohort as a survival predictor. (A) Hierarchical clustering of 68 Caucasian ICC cases based on the expression of 158 overlapping genes between stem-like ICC and stem-like HCC genes using centered correlation and average linkage. The heatmap depicts high (red) and low (green expression of these genes based on a log2 scale. (B) Kaplan-Meier plot of 68 ICC patients based on the dendrogram classification from (A).

cell-like phenotype. We plotted the density distribution of Spearman correlation coefficients of 636 experimentally derived genes and 23 experimentally derived microRNAs (Fig. 4A). This analysis revealed that there was a clear enrichment of correlative mRNA-microRNA pairs derived from these signatures because a positive correlative curve shifted to the right and a negative correlative curve shifted to the left when compared to a normal distribution curve derived from a global correlation of all available mRNA and microRNA probes (Fig. 4A). A correlation coefficient of 0.5, corresponding to the 95th percentile of the 100-fold random permutations, was used as the cutoff threshold for positive correlation. These results indicated that ICC-specific mRNAs and microRNAs are enriched in the experimentally derived signatures and they are highly correlated.

To determine if there is any enrichment of affected networks associated with ICC subgroups, we combined significantly correlative mRNA-microRNA pairs and performed pathway analysis using Ingenuity Pathway Analysis (IPA, v. 9.0) that incorporates microRNA-mRNA target relationships from TargetScan. Among 1,077 mRNA-microRNA pairs identified by this analysis, 479 pairs showed negative correlation. Among the top nine networks (Table S4), five microRNAs including miR-200c and miR-141 that are encoded by the same transcript were negatively correlated with genes

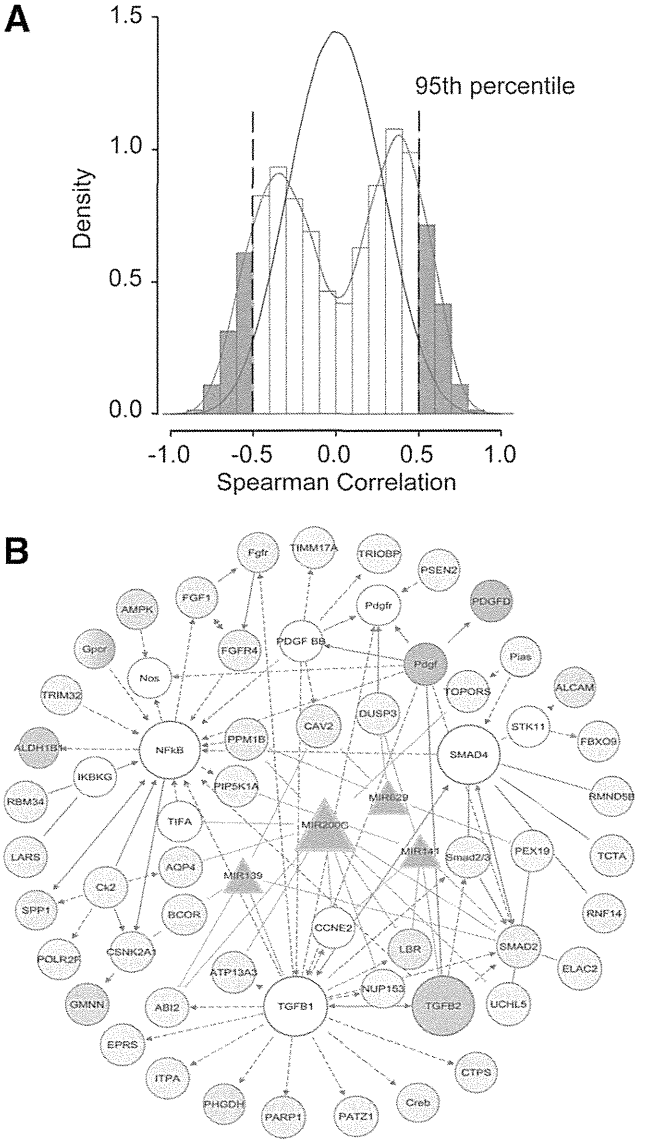

Fig. 4. Integrative analyses of ICC-specific mRNA and microRNAs based on Spearman correlation and ingenuity pathway. (A) Correlation between ICC-specific 636 mRNA and 23 microRNA signatures. (B) The top nine gene networks of signaling including TGF-β, Smad4, and NF-κB pathways activated in stem-like ICC tumors. Red shaded ovals represent up-regulated genes in HpSC-ICC tumors, and open ovals represent genes that are not on the list of significant genes but are reported to be associated with the network. Blue shaded triangles represent down-regulated microRNAs specific to HpSC-ICC tumors. The open ovals that are labeled TGF-β, Smad4, and NF-κB represent molecular nodes related to their respective signaling pathways. Arrows represent positive regulation of gene expression, with solid arrows indicating direct regulation and broken arrows indirect regulation. Blue lines connecting between microRNA and genes represent direct targeting predicted by TargetScan.

in the transforming growth factor beta (TGF-β), nuclear factor kappa B (NF-κB), and Smad signaling pathways (Fig. 4B). A common link between ICC-specific mRNA and microRNA seemed to be related to EMT, where all three pathways are known regulators. Consistently, known stem cell-related genes such as POU5F1 (Oct4), NANOG, NCAM1, and PROM1 (CD133) were much more abundantly expressed in HpSC-ICC than MH-ICC cases (Fig. S5A). TGFB1 was also significantly elevated in HpSC-ICC compared to MH-ICC. However, no difference in EpCAM expression was observed among these two subgroups. An elevated expression of NCAM1 and TGFB1 in a majority of HpSC-ICC cases was confirmed by immonohistochemistry analysis (IHC) (Fig. S5B).

Among the affected networks, it was noticeable that miR-200c appeared a common molecular note linking to EMT, as it had a direct interaction with many of the affected genes in this pathway (Fig. 4B). Consistently, the expression level of miR-200c was associated with overall survival and disease-free survival in ICC cases (Fig. S6). These data suggested that miR-200c may play an important role in maintaining HpSC-like phenotype.

To determine whether EMT was functionally linked to HpSC-ICC cells, we first analyzed representative expression levels of EMT markers in ICC specimens by qRT-PCR. Consistently, mesenchymal markers such as ZEB1, ZEB2, CDH2, and VIM were more abundantly expressed, whereas an epithelial marker, CDH1, and miR-141/miR-200c were much less abundantly expressed in HpSC-ICC cases as compared to MH-ICC cases (Fig. 5A). Next, we determined if an altered miR-200c expression could lead to EMT in ICC cells. We selected two ICC cell lines that represent two opposite ends of the EMT spectrum. A nonmalignant H69 cell line derived from normal human intrahepatic cholangiocytes was included as a control.[24] HuH28 cells had fibroblast-like cell morphology with mesenchymal appearances and expressed very low levels of miR-200c but high levels of mesenchymal markers, whereas HuCCT1 cells had cobblestone-like cell morphology with epithelial appearances and expressed high levels of miR-200c but low levels of mesenchymal markers (Fig. 5B). The miR-200c level was also relatively high in H69 cells with epithelial morphology. Transient transfection of miR-200c oligos in HuH28 cells induced a reversed EMT from a mesenchymal-like to a cobblestone-like morphology with a suppression of genes that mediate EMT (Fig. 5C). Conversely, transfection of an anti-miR-200c oligo in HuCCT1 resulted in an induction of mesenchymal markers (Fig. 5D). In addition, overexpression of miR-200c suppressed cell migration (Fig. 5E) and invasion (Fig. 5F) in HuH28 cells. However, miR-200c did not affect cell proliferation and apoptosis in HUH28 cells as measured by 3-(4,5-dimethylthiazol-2-yl)-2,5-diphenyltetrazolium bromide (MTT) and Transferase-Mediated dUTP Nick-End Labeling (TUNEL) assays (Fig. S7).

Analyses of the genomic region encoding the human miR-200c/miR-141 locus at the UCSC Genome Browser revealed that miR-200c and miR-141 are derived from a single transcript encoded by a predicted gene (ENST00000537269) (Fig. 6A). The available Chip-Seq data revealed several transcriptional factors such as c-Myc and TCF4 to be preferentially bound to the immediate 5′ upstream sequence of the predictive transcription initiation site. To determine whether c-myc directly regulates miR-200c expression, we silenced c-Myc expression with a c-myc-specific small interfering RNA (siRNA) in HuH28 cells and examined the activity of a luciferase reporter containing an upstream 0.9 kb fragment of pri-miR-200c[25] (Fig. 6B). Consistently, we found that inhibition of c-Myc resulted in an increased hmiR-200cLuc activity. Moreover, c-myc siRNA could effectively induce endogenous miR-200c expression, however suppress mesenchymal markers but induce epithelial marker (Fig. 6C).

NCAM1 as a Direct Target of MiR-200c. Because several stem/progenitor cell-related genes such as POU5F1, NANOG, MYC, TGFB1, NCAM1, and PROM1 are overexpressed in HpSC-ICC cases (Fig. S5), we reasoned that some of these genes may be targets of miR-200c. TargetScan analysis (TargetScanHuman 6.0) revealed that only NCAM1 contained a classical and evolutionarily conserved miR-200c binding site at its 3′ untranslated region (UTR) (Fig. 7A). Ectopic expression of miR-200c in HuH28 cells resulted in a reduction (Fig. 7B), whereas inhibition of miR-200c in HuCCT1 cells led to an increased expression of NCAM1 (Fig. 7C). To further determine whether NCAM1 was a bona fide target of miR-200c-mediated silencing, the miR-200c binding site was cloned into a luciferase reporter. We found that forced expression of miR-200c in HUH28 cells resulted in decreased luciferase activity when a wildtype sequence but not a mutant sequence was present (Fig. 7D). Moreover, inhibition of miR-200c in HuCCT1 cells resulted in increased luciferase activity only from a wildtype reporter (Fig. 7E). Consistently, ICC cases with high levels of NCAM1 had a worse survival compared to those with low NCAM1 expression (Fig. 7F). Moreover, a significant inverse correlation was observed between miR-200c and NCAM1 (Fig. 7G).

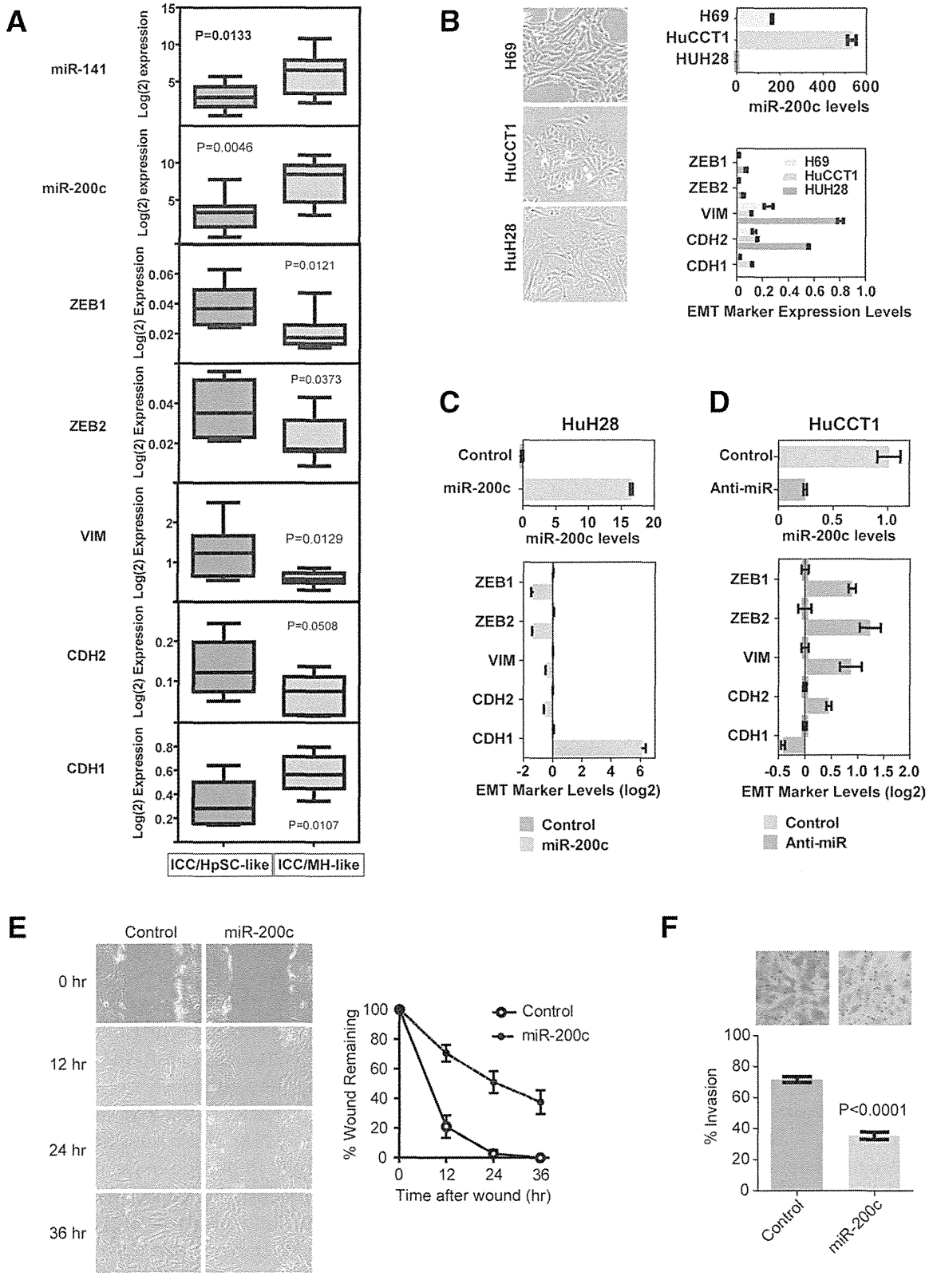

Fig. 5. Inactivation of miR-200c/miR-141 and activation of EMT-related genes are associated with stem-like ICC. (A) Expression analyses of miR-141/miR-200c transcripts and EMT-specific markers based qRT-PCR data in eight HpSC-ICC and eight MH-ICC samples classified by gene clustering from Fig. 1. The horizontal lines in the boxplots represent the median, the boxes represent the interquartile range, and the whiskers represent the 10th and 90th percentiles. A nonparametric test was used to compare the two groups and *P* values are indicated. (B) Expression of miR-200c and EMT-specific genes in HuH28, HuCCT1, and H69 cells as analyzed by qRT-PCR. (C) Expression of EMT-specific genes in HuH28 cells transduced with miR-200c as analyzed by qRT-PCR. (D) Expression of EMT-specific genes in HuCCT1 cells transduced with an anti-miR-200c oligo as analyzed by qRT-PCR. (E) Cell migration of HuH28 cells transduced with miR-200c as determined by the wound healing assay. (F) Cell invasion of HuH28 cells transduced with miR-200c as determined by the Boyden chamber cell invasion assay. Representative images are shown.

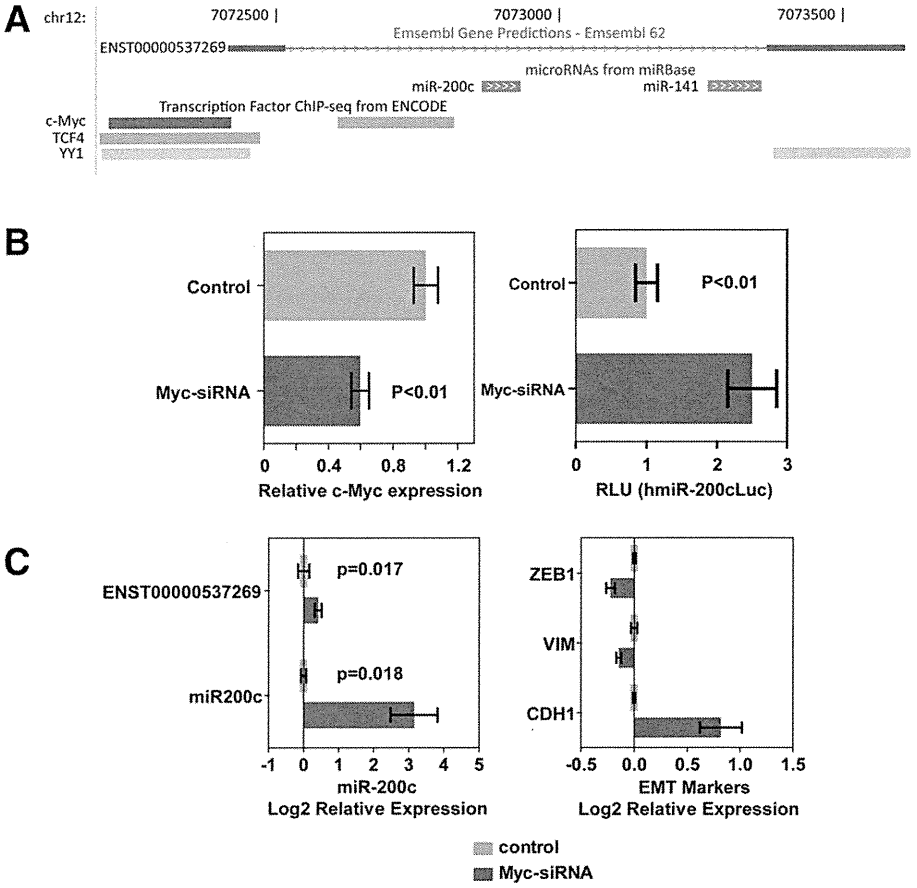

Fig. 6. c-Myc-mediated silencing of miR-200c and induction of EMT. (A) The genome position of ENST00000537269 encoding miR-200c and miR-141, based on Ensembl Gene Predictions using UCSC Genome Browser. (B) Effect of c-Myc siRNA on miR-200cc-Myc expression (left panel) and the miR-200c promoter luciferase activity (right panel) in HuCCT1 cells. (C) Effect of c-Myc siRNA on endogenous levels of miR-200c and induction of EMT-related gene expression in HuCCT1 cells.

Discussion

Similar to HCC, ICC is heterogeneous in clinical presentation, although our knowledge related to its tumor biology is limited. Several recent studies have begun dissecting the molecular pathogenesis of ICC including functional roles of microRNA in ICC cells.[27,28] Recently, we used global transcriptomic approaches to study HCC heterogeneity and identified critical genetic loci functionally linked to hepatic CSCs with gene expression profiles resembling normal hepatic stem cells.[7,8] We also used these approaches to study cholangiocarcinoma.[15,23] In this study, we examined whether ICC and HCC are distinct at the transcriptomic levels. Using two independent transcriptomics approaches, we found that ICC cases from Asian patients can be mainly divided into two subgroups with one resembling of stem-like HCC and other mature hepatocyte-like HCC. Consistently, we found that several known hepatic stem/progenitor cell-specific genes such as POU5F1 (Oct4), NANOG, MYC, TGFB1, NCAM1, and PROM1 are more abundantly expressed in stem-like ICC than mature hepatocyte-like ICC.[29] Moreover, both ICC-specific mRNA and microRNA signatures could independently predict HCC survival as well as ICC prognosis in Caucasian patients. These results are consistent with our recent finding that a subset of HCC may share an ICC-like gene expression trait.[15] Integrative pathway analyses revealed that an altered miR-200c signaling pathway linked to EMT may be responsible for the maintenance of stem-like ICC associated with poor prognosis. For example, we found that two significant microRNAs, i.e., miR-200c and miR-141, encoded by the same transcript, were negatively correlated with genes in the TGF-β, NF-κB, and Smad signaling pathways. These two microRNAs share the same seed sequences and are predicted to have similar cellular functions. EMT is an important biological process contributing to embryogenesis and organ development.[30] Recently, components of EMT have been shown to be critical in promoting cancer invasion and metastasis.[31] TGF-β is essential for the induction of EMT during various stages of embryogenesis and plays an important role in carcinoma progression into an invasive state.[32-34] Smad signaling is essential for TGF-β-induced EMT.[35] Furthermore, miR-200 family members including miR-141 and miR-200c induce epithelial differentiation, thereby suppressing EMT by inhibiting translation of mRNA for the EMT-activators ZEB1 and